Int. J. Electrochem. Sci., 8 **(2013)** 3419 - 3428

International Journal of
ELECTROCHEMICAL
SCIENCE
www.electrochemsci.org

Phase Structure and Electrochemical Hydrogen Storage Characteristics of $La_{0.7}Ce_{0.3}Ni_{3.85}Mn_{0.8}Cu_{0.4}Fe_{0.15-x}(Fe_{0.43}B_{0.57})_x$ (x = 0-0.15) Alloys

Xianyun Peng[1], *Baozhong Liu*[1,*], *Yanping Fan*[1], *Liqiang Ji*[2], *Baoqing Zhang*[2], *Zhi Zhang*[1]

[1] School of Materials Science & Engineering, Henan Polytechnic University, Jiaozuo 454000, China
[2] Inner Mongolia Rare Earth Ovonic Metal Hydride Co. Ltd., Baotou 014030, China
[*]E-mail: bzliu@hpu.edu.cn

Received: 2 January 2013 / *Accepted:* 8 February 2013 / *Published:* 1 March 2013

Phase structure and electrochemical hydrogen storage performance have been investigated. XRD results indicate that $La_{0.7}Ce_{0.3}Ni_{3.85}Mn_{0.8}Cu_{0.4}Fe_{0.15}$ alloy is single $LaNi_5$ phase with $CaCu_5$ structure. The alloys containing $Fe_{0.43}B_{0.57}$ are composed of $LaNi_5$ phase with $CaCu_5$ structure as matrix phase and $La_3Ni_{13}B_2$ phase as secondary phases, and the abundance of the secondary phase gradually increases with increasing $Fe_{0.43}B_{0.57}$ content. As x increases from 0 to 0.15, maximum discharge capacity of the alloy electrodes monotonically decreases from 314.7 to 300.1 mAh/g. High-rate dischargeability at the discharge current density of 1200 mA/g increases from 53.3% (x = 0) to 64.4% (x = 0.15) with increasing x value. Cycling stability of the alloy electrodes decreases with increasing x value.

Keywords: Hydrogen storage alloys; X-ray diffraction topography; Microstructure; Electrochemical properties; Ni/MH battery

1. INTRODUCTION

With respect to the recent increasing demand for the high performance of secondary batteries and for environmental protection, nickel/metal hydride (Ni/MH) rechargeable batteries using hydrogen storage alloy as a negative electrode materials have drawn much attention because they have several advantages over the conventional secondary batteries, such as good activation ability, high capacity, high resistance to overcharging and over-discharging, capable of performing a high rate charge/discharge, long cycle life and environmental friendliness, ect [1-3]. However, wide application of Ni/MH battery is hindered due to the high cost of negative electrode materials. In order to decrease the raw cost, lots of Co-less or Co-free alloys were prepared by substituting Co with foreign metals,

such as, Fe, Cu, Si, etc, whose raw cost are much cheaper than Co [4-6]. Co-free alloy with high Mn content were developed and commercially produced [7]. However, the electrochemical performances, especially high-rate dischargeability, of Co-free alloy with high Mn content are not still satisfying. Thus, it is necessary to further improve the high-rate dischargeability of the Co-free high-Mn alloy without increasing the raw cost.

Ye et al. [8] reported that the addition of boron significantly improved the high-rate capacity and modified the activation performance of $Mm_{3.55}Co_{0.75}Mn_{0.4}Al_{0.3}B_x$ alloy though the electrochemical capacity was lower than that of commercial $Mm_{3.55}Co_{0.75}Mn_{0.4}Al_{0.3}$ alloy. Zhang et al. [9] studied hydrogen storage properties of $MmNi_{3.8}Co_{0.4}Mn_{0.6}Al_{0.2}B_x$ alloys and pointed out that the addition of B enhanced the cycling stability, activation performance and high-rate discharge capability. Yang et al. [10] found that the substitution of B for Ni in $MmNi_{3.70-x}Mn_{0.35}Co_{0.60}Al_{0.25}B_x$ hydrogen storage alloys improved the activation ability and the high-rate dischargeability of the alloy electrodes. The addition of B element has been proved to be effective to enhance the activation performance and the high-rate dischargeability. Therefore, it can be expected that the high-rate dischargeability and activation property could be improved by substitution of B for Fe in AB_5-type hydrogen storage alloys. However, pure B is very expensive and unpractical to be used in Co-less or Co-free alloys. Fortunately, the cost of commercial $Fe_{0.43}B_{0.57}$ alloy is obviously lower than that of pure B, and the $Fe_{0.43}B_{0.57}$ alloy has much lower melt point than that of pure B, and then facilitates the homogeneity. In addition, Ye et al. [11] have reported that Fe-B can replace B as additive in $MmNi_{3.55}Co_{0.75}Mn_{0.4}Al_{0.3}B_{0.3}$ alloy without the significant decrease in high-rate dischargeabiltiy. Yan et al. [12] have developed multiphase La-Fe-B alloy with good activation property and high-rate dischargeability. Thus, it is feasible and promising to substitute Fe using $Fe_{0.43}B_{0.57}$ rather than pure B in Co-free high-Mn alloy.

In this work, on the basis of the merits of $Fe_{0.43}B_{0.57}$ and the belief that the substitution of Fe by B may result in some noticeable modification of hydrogen storage properties, phase structure and electrochemical hydrogen storage properties of $La_{0.7}Ce_{0.3}Ni_{3.85}Mn_{0.8}Cu_{0.4}Fe_{0.15-x}(Fe_{0.43}B_{0.57})_x$ (x = 0-0.15) alloys have been investigated systematically.

2. EXPERIMENTAL PROCEDURES

$La_{0.7}Ce_{0.3}Ni_{3.85}Mn_{0.8}Cu_{0.4}Fe_{0.15-x}(Fe_{0.43}B_{0.57})_x$ (x = 0-0.15) alloys were synthesized by induction melting of the metal elements (La, Ce, Ni, Mn, Fe, Cu: 99.9% purity and FeB alloy contained 57.0% B and the other were Fe and trace impurities.) under argon atmosphere and then were annealed at 1223 K for 10 h under argon atmosphere with the pressure of 0.08 MPa.

The phases of the alloy powders were determined by X-ray diffraction (XRD) using a Rigaku D/max 2500PC powder diffractometer with Cu Kα radiation. The phase structures of the alloys were analyzed using Jade-5 software.

All the alloy electrodes for test were prepared by cold pressing the mixture of 0.15 g alloy powders of 200-400 meshes and 0.75 g nickel carbonyl powders into a pellet of 10 mm in diameter under 15 Mpa. Electrochemical measurements were performed at 298 K in a standard tri-electrode system, consisting of a working electrode (metal hydride), a counter electrode ($Ni(OH)_2$/NiOOH), and

a reference electrode (Hg/HgO) with 6mol/L KOH solution as electrolyte. Each electrode was charged for 7 h at 60 mA/g and discharged to -0.6 V versus Hg/HgO at 60 mA/g at 298 K. After every charging/discharging, the rest time was 10 min. In evaluating the high-rate dischargeability, discharge capacity of the alloy electrode at different discharge current density were measured. The high-rate dischargeability HRD (%) was defined as $C_d/C_{max} \times 100\%$, where C_d was the discharge capacity at the discharge current density I_d (I_d = 60, 300, 600, 900 and1200 mA/g) and C_{max} was the maximum discharge capacity at the discharge current density I_d = 60 mA/g.

The linear polarization curve and potential-step measurement were obtained by Advanced Potentiostat/Galvanostat (PARSTAT 2273), respectively. At 50% depth of discharge (DOD), the linear polarization curve was obtained by scanning the electrodes from - 5 to 5 mV (vs. open circuit potential). For potential-step measurement, the electrodes in fully charged state were discharged with potential steps of 0.5 V for 3600 s.

3. RESULTS AND DISCUSSION

3.1 Crystal structure

Fig. 1 presents XRD patterns of $La_{0.7}Ce_{0.3}Ni_{3.85}Mn_{0.8}Cu_{0.4}Fe_{0.15-x}(Fe_{0.43}B_{0.57})_x$ alloys. It can be seen that $La_{0.7}Ce_{0.3}Ni_{3.85}Mn_{0.8}Cu_{0.4}Fe_{0.15}$ alloy is single $LaNi_5$ phase with $CaCu_5$ structure, and the alloys containing $Fe_{0.43}B_{0.57}$ consist of two phases, $LaNi_5$ matrix phase and $La_3Ni_{13}B_2$ secondary phase. The abundance of $La_3Ni_{13}B_2$ phase increases with the increase of x value. Calculated lattice parameters of $LaNi_5$ phase in all alloys are listed in Table 1. Clearly lattice constant a, c and cell volume V decrease with increasing x value, and c/a ratio of $LaNi_5$ phase also decreases with the increase of x value.

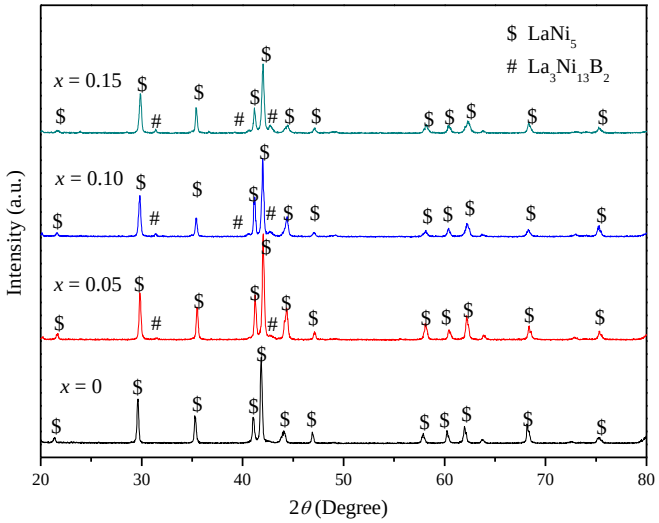

Figure 1. XRD patterns of $La_{0.7}Ce_{0.3}Ni_{3.85}Mn_{0.8}Cu_{0.4}Fe_{0.15-x}(Fe_{0.43}B_{0.57})_x$ alloys

Table 1. Lattice parameters of $La_{0.7}Ce_{0.3}Ni_{3.85}Mn_{0.8}Cu_{0.4}Fe_{0.15-x}(Fe_{0.43}B_{0.57})_x$ alloys

x	a/Å	c/Å	c/a	V/Å^3
0	5.0676	4.1234	0.81368	91.701
0.05	5.0571	4.1032	0.81137	90.875
0.10	5.0565	4.0973	0.81030	90.723
0.15	5.0487	4.0875	0.80961	90.227

3.2 Activation capability and discharge capability

The number of cycles (N_a) needed to activate the electrodes and maximum discharge capacity (C_{max}) of $La_{0.7}Ce_{0.3}Ni_{3.85}Mn_{0.8}Cu_{0.4}Fe_{0.15-x}(Fe_{0.43}B_{0.57})_x$ alloy electrodes are given in Table 2. It is noted that N_a decreases with increasing x value, indicating increasing B content and decreasing Fe content contribute to the activation properties of alloy electrode. Generally, the activation performance of the alloy electrode is related to surface characteristics and phase structure of the alloy [13]. Firstly, the formation of the secondary phase increased the number of phase boundaries, which provided extra tunnels for the diffusion of hydrogen atoms and was buffer area of the releasing of the stress formed in the process of hydrogen absorbed [14,15]. The increase of $La_3Ni_{13}B_2$ secondary phase causes the increase in the phase boundary, which can decrease the lattice distortion and strain energy formed in the process of hydrogen absorption, and then contributes to the activation property. Secondly, Due to the low surface energy of Fe, the oxidation of Fe on the alloy surface forms easily. The oxidation film becomes thin with decreasing x value, which is also favorable to activation property. The C_{max} of alloy electrodes monotonically decreases from 314.7 mAh/g (x = 0) to 300.1 mAh/g (x = 0.15), indicating Fe substation by B is detrimental to the maximum discharge capacity. The discharge capacity of $La_3Ni_{13}B_2$ phase is 157 mAh/g [16], which is much lower than that of $LaNi_5$ matrix phase. The abundant of $La_3Ni_{13}B_2$ phase increases with increasing x value according to XRD results, therefore increasing x value is unfavorable for discharge capability. Moreover, Brateng et al. [17] pointed out that the discharge capacity has a linear relationship with the cell volume. The larger cell volume is, the discharge capacity is higher. The decrease in cell volume of $LaNi_5$ matrix phase with increasing x value is detrimental to the discharge capacity. On the other hand, the decrease of Fe content results in the decrease of surface oxide film, which will contribute to the charge-transfer reaction on the alloy surface, which is favorable to the discharge performance. As mentioned above, the increase of $La_3Ni_{13}B_2$ secondary phase causes the increase in the phase boundary, which can provide more hydrogen diffusion channel, and then improve the kinetics. This is beneficial to the discharge property. Thus, it is reasonable that the unfavorable factors are prominent for the decrease of the C_{max} of $La_{0.7}Ce_{0.3}Ni_{3.85}Mn_{0.8}Cu_{0.4}Fe_{0.15-x}(Fe_{0.43}B_{0.57})_x$ alloy electrodes.

Table 2. Electrochemical properties of $La_{0.7}Ce_{0.3}Ni_{3.85}Mn_{0.8}Cu_{0.4}Fe_{0.15-x}(Fe_{0.43}B_{0.57})_x$ alloy electrodes

x	C_{max} (mAh/g)	N_a	HRD_{1200} [a] (%)	S_{100} (%)
0	314.7	4	53.3	76.6
0.05	308.4	3	56.5	65.2
0.10	303.3	2	60.9	53.4
0.15	300.1	2	64.4	49.2

[a] The high-rate dischargeability at the discharge current density of 1200 mA/g.

3.4 High-rate dischargeability and electrochemical kinetics

Fig. 3 shows the relationship between the high-rate dischargeability (HRD) and the discharge current density of $La_{0.7}Ce_{0.3}Ni_{3.85}Mn_{0.8}Cu_{0.4}Fe_{0.15-x}(Fe_{0.43}B_{0.57})_x$ alloy electrodes. The HRD of the alloy electrodes increases with increasing x from 0 to 0.15.The HRD at the discharge current density of 1200 mA/g is listed in Table 2. It can be seen that HRD_{1200} increases from 53.3% (x = 0) to 64.4% (x = 0.15).

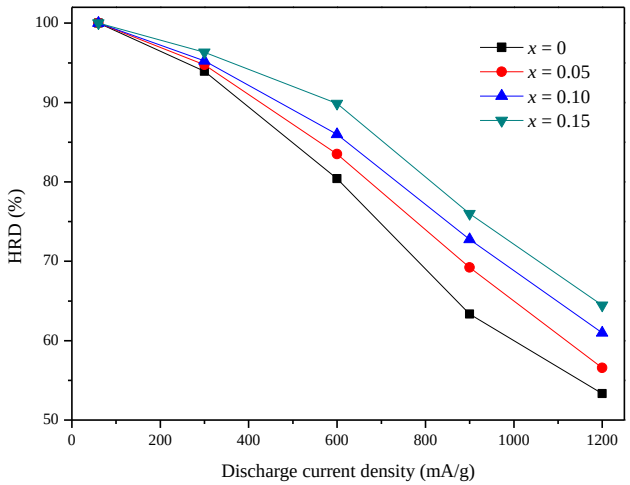

Figure 2. HRD of $La_{0.7}Ce_{0.3}Ni_{3.85}Mn_{0.8}Cu_{0.4}Fe_{0.15-x}(Fe_{0.43}B_{0.57})_x$ alloy electrodes

It is well known that the HRD of the MH electrodes is dominated by the electrochemical kinetics of the charge-transfer reaction at the electrode/electrolyte interface and the hydrogen diffusion rate within the bulky alloy electrode, which are reflected in the value of the charge-transfer resistance (R_{ct}) and/or surface exchange current density (I_0), being a measure of the catalytic activity of an alloy, as well as in the hydrogen diffusion coefficient (D), which characterizes the mass transport properties of an alloy electrode [18].

Fig. 5 shows the linear polarization curves of $La_{0.7}Ce_{0.3}Ni_{3.85}Mn_{0.8}Cu_{0.4}Fe_{0.15-x}(Fe_{0.43}B_{0.57})_x$ alloy electrodes at 50% DOD and 298 K. The polarization resistances (R_p) are calculated through

estimating the slopes of linear polarization curves, and listed in Table 3. The R_p values of the alloy electrodes decreases from 255.5 mΩ g (x = 0) to 187.7 mΩ g (x = 0.15). Besides, the exchange current density I_0 can also describe the charge-transfer process. The I_0 value can be calculated according to the following formula [19].

$$I_0 = \frac{RT}{FR_p} \qquad (1)$$

where R, T, F, R_p are the gas constant, the absolute temperature, the Faraday constant and the polarization resistance, respectively. The I_0 values are calculated by Eq. (1) and listed in Table 3. It is clear that the I_0 increases from 100.5 (x = 0.00) to 136.8mA/g (x = 0.15). It is reported that the formation of the secondary phase improves the catalytic activity of the alloys [10-12]. As mentioned above, the secondary phase $La_3Ni_{13}B_2$ increases with increasing x value, which is beneficial to the electrocatalytic activity of the surface of alloy electrode and improves the charge-transfer reaction. Moreover, decreasing Fe will cause the decrease of surface oxide film and then improve the charge-transfer reaction on the alloy surface.

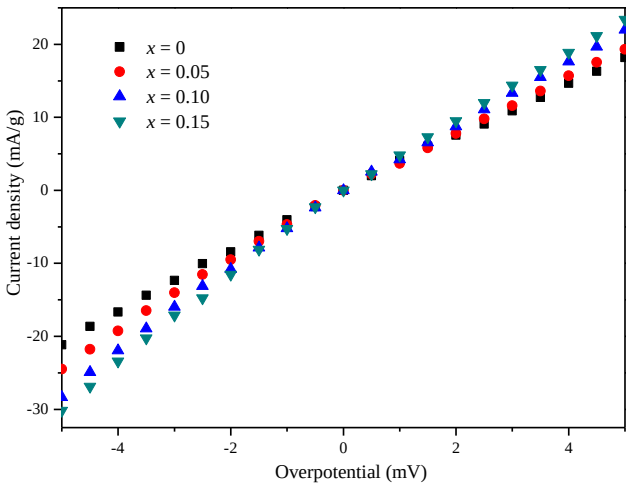

Figure 3. Linear polarization of $La_{0.7}Ce_{0.3}Ni_{3.85}Mn_{0.8}Cu_{0.4}Fe_{0.15-x}(Fe_{0.43}B_{0.57})_x$ alloy electrodes

The diffusion coefficient of hydrogen in the alloy electrodes is determined with the potential-step method. Fig. 6 shows the semi-logarithmic plots of the anodic current vs. the time response of the $La_{0.7}Ce_{0.3}Ni_{3.85}Mn_{0.8}Cu_{0.4}Fe_{0.15-x}(Fe_{0.43}B_{0.57})_x$ alloy electrodes. Zheng et al. [20] have reported that MH electrode reaction would be controlled by the rate of hydrogen diffusion in the bulk of alloys, when the rate of charge-transfer on the surface of alloy electrodes was so fast that the hydrogen concentration nearly equal to zero under a large anodic potential-step. Assuming that the grains of alloys are all spherical， and the initial hydrogen concentration in the bulk of the alloy is uniform and the hydrogen surface concentration is constant. When the discharge time is long enough, the hydrogen diffusion

coefficient D can be calculated by the slope from the linear plot of lg (i) versus t using the following formula.

$$\lg i = \lg\left(\frac{6FD}{da^2}(C_0 - C_s)\right) - \frac{\pi^2}{2.303}\frac{D}{a^2}t \qquad (2)$$

where i is anodic current density (A/g), D the hydrogen diffusion coefficient (cm^2/s), d the density of the alloy (g/cm^3), a the radius of the alloy particle, C_0 the initial hydrogen concentration in the bulk of the alloy (mol/cm^3), C_s the surface hydrogen concentration of the alloy (mol/cm^3) and t is the discharge time (s). Assuming that the alloy powders have a similar particle distribution with an average particle radius of 13 μm, and D is calculated according to the formula above and summarized in Table 3. The D of $La_{0.7}Ce_{0.3}Ni_{3.85}Mn_{0.8}Cu_{0.4}Fe_{0.15-x}(Fe_{0.43}B_{0.57})_x$ alloy electrodes increases from 7.84 $\times 10^{-11}$ (x = 0.00) to 8.18 $\times 10^{-11}$ cm^2/s (x = 0.15), which should be ascribed to following factors. Firstly, the phase boundary of the secondary phase $La_3Ni_{13}B_2$ increasing is favorable for hydrogen diffusion. Secondly, it is also claimed that the stability of metal hydride gradually decreases with increasing B content [10]. The increase of B content will lower the stability of the alloy hydride and then cause the hydrogen desorption easily, which contributed to hydrogen diffusion. Thirdly, Iwakura et al. [21] have reported that the oxidation of Fe on the alloy surface limited the hydrogen transfer from the surface to the bulk of the alloys. As mentioned above, the decrease of Fe content causes the decrease of surface oxide film, which is beneficial to the hydrogen diffusion.

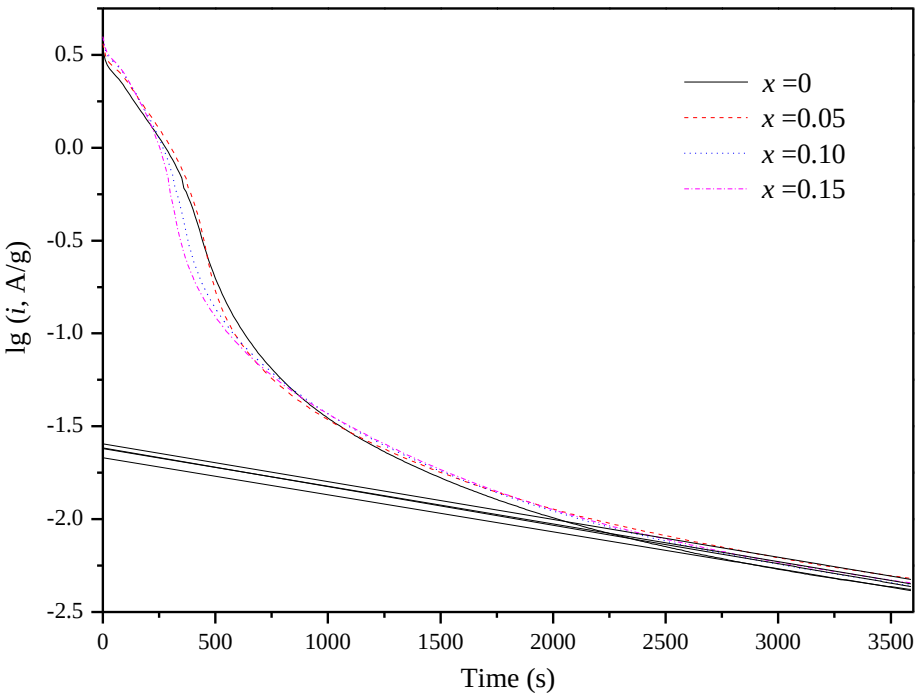

Figure 4. Semilogarithmic curves of anodic current vs. time response of $La_{0.7}Ce_{0.3}Ni_{3.85}Mn_{0.8}Cu_{0.4}Fe_{0.15-x}(Fe_{0.43}B_{0.57})_x$ alloy electrodes

Table 3. Electrochemical kinetic characteristics of $La_{0.7}Ce_{0.3}Ni_{3.85}Mn_{0.8}Cu_{0.4}Fe_{0.15-x}(Fe_{0.43}B_{0.57})_x$ alloy electrodes

x	R_{ct} (mΩ g)	I_0 (mA/g)	D ($\times 10^{-11}$ cm^2/s)
0	255.5	100.5	7.84
0.05	229.6	111.8	7.98
0.10	201.3	127.6	8.10
0.15	187.7	136.8	8.18

Iwakura et al. [22] have reported that linear dependence of the HRD on exchange current density and activation energy of hydrogen diffusion indicated that the charge transfer and hydrogen diffusion are responsible for discharge efficiency. Fig. 7 shows the HRD_{1200} as a function of the I_0 and the D of $La_{0.7}Ce_{0.3}Ni_{3.85}Mn_{0.8}Cu_{0.4}Fe_{0.15-x}(Fe_{0.43}B_{0.57})_x$ alloy electrodes. It is evident that the HRD_{1200} increases with the increase of the I_0 and the D, and shows a linear relationship with the I_0 and the D, respectively. This implies that both charge-transfer reaction at the electrode/electrolyte interface and the hydrogen diffusion of alloy electrodes should be responsible for the HRD at a discharge current density of 1200 mA/g.

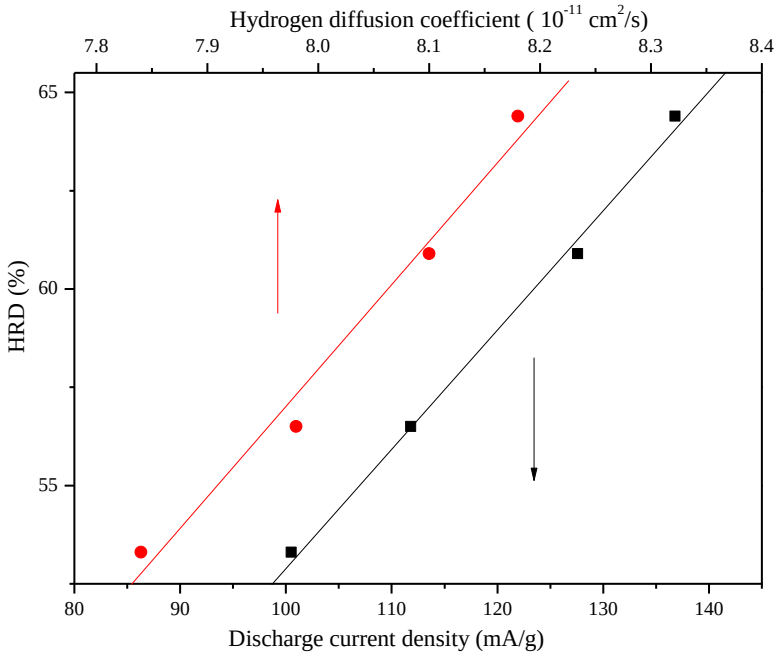

Figure 5. HRD at 1200 mA/g as a function of exchange current density for $La_{0.7}Ce_{0.3}Ni_{3.85}Mn_{0.8}Cu_{0.4}Fe_{0.15-x}(Fe_{0.43}B_{0.57})_x$ alloy electrodes

3.4 Cycling stability

The cycle stability is an extremely important factor for the service life of a hydrogen storage alloy. The discharge capacity of the alloy electrode as a function of cycle number is shown in Fig. 2.

The cycling capacity retention rate, expressed as $S_n(\%) = C_n/C_{max} \times 100$ (where C_n is the discharge capacity at the nth cycle), is listed in Table 1. It can be seen that S_{100} decreases from 76.6% (x = 0) to 49.2% (x = 0.15). It is confirmed that the fundamental reasons for the capacity decay of the electrode alloy are alloy corrosion and the pulverization of the alloy during charge-discharge cycle [23]. As is well-known that pulverization of AB_5-type metal hydrides during absorption/desorption of hydrogen is an inherent problem that is resulted from the combination of volume change and their brittle nature. The increase in c/a ratio of main-phase facilitates hydrogen atoms from going in and out of the crystal and therefore decreases lattice stress during charging/discharging cycles [24]. The c/a ratio of $LaNi_5$ phase decreases with increasing x value, which will increase lattice stress and decrease pulverization resistance. On the other hand, the oxidation of Fe on the alloy surface forms easily due to the low surface energy of Fe. The decreasing of Fe is beneficial to the corrosion resistance with increasing x value. Thus, it is reasonable to believe that the decrease of pulverization resistance is prominent for the degradation of cycling stability of $La_{0.7}Ce_{0.3}Ni_{3.85}Mn_{0.8}Cu_{0.4}Fe_{0.15-x}(Fe_{0.43}B_{0.57})_x$ alloy electrodes in present work.

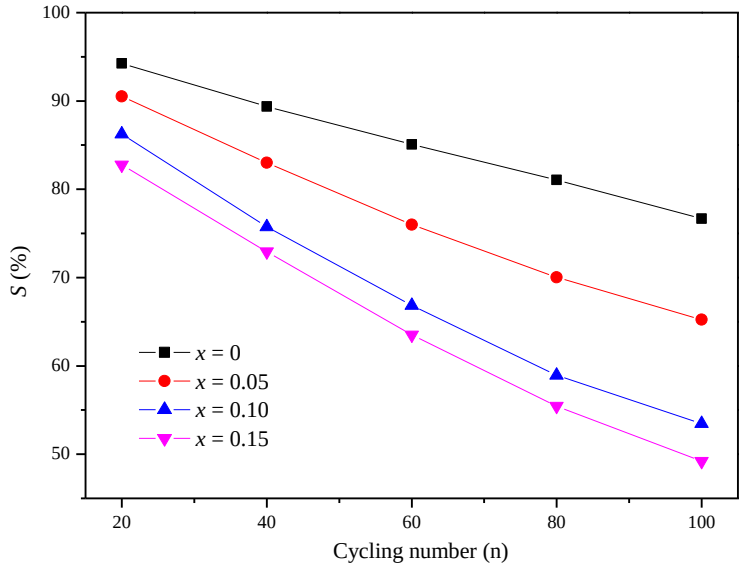

Figure 6. Cycling stability of $La_{0.7}Ce_{0.3}Ni_{3.85}Mn_{0.8}Cu_{0.4}Fe_{0.15-x}(Fe_{0.43}B_{0.57})_x$ alloy electrodes

4. CONCLUSIONS

Phase structure and electrochemical properties of Co-free $La_{0.7}Ce_{0.3}Ni_{3.85}Mn_{0.8}Cu_{0.4}Fe_{0.15-x}(Fe_{0.43}B_{0.57})_x$ (x = 0-0.15) alloys have been investigated. XRD indicates that $La_{0.7}Ce_{0.3}Ni_{3.85}Mn_{0.8}Cu_{0.4}Fe_{0.15}$ alloy consists of a single $LaNi_5$ phase with $CaCu_5$ structure. The alloys containing $Fe_{0.43}B_{0.57}$ are composed of $LaNi_5$ phase with $CaCu_5$ structure as matrix phase and $La_3Ni_{13}B_2$ phase as secondary phases, and the abundance of the secondary phase gradually increases with increasing $Fe_{0.43}B_{0.57}$ content. Maximum discharge capacity of the alloy electrodes monotonically decreases from 314.7 mAh/g (x = 0) to 300.1 mAh/g (x = 0.15) with the crease of x value. High-rate dischargeability at the discharge current density of 1200 mA/g increases from 53.3% (x = 0) to 64.4%

(x = 0.15), and HRD_{1200} increases with the increase of the I_0 and the D, and shows a linear relationship with the I_0 and the D. Cycling stability of the alloy electrodes decreases with increasing x value, which is ascribed to the decrease of pulverization resistance.

ACKNOWLEDGEMENTS
This research is financially supported by the National Natural Science Foundation of China (51001043), Program for New Century Excellent Talents in University (NECT2011), China Postdoctoral Science Special Foundation (201104390), China Postdoctoral Science Foundation (20100470990), Program for Innovative Research Team (in Science and Technology) in the University of Henan Province (2012IRTSTHN007), Baotou Science and Technology Project **(**2011J1003) and the Doctoral Foundation of Henan Polytechnic University (B2010-13).

References

1. T. Sakai, H. Yoshinaga, H. Migamura, N. Kurigama, H. Ishikawa, *J. Alloys Compd.*, 180 (1992) 37
2. Y. Fukumoto, M. Miyamoto, M. Matsuoka, C. Iwakura, *Electrochim. Acta*, 40 (1995) 845
3. S. Bliznakov, E. Lefterova, N. Dimitrov, K. Petrov, A. Popov, *J. Power Sources*, 176 (2008) 381
4. C. Khaldi, H. Mathlouthi, J. Lamloumi, A. Percheron-Guégan, *Int. J. Hydrogen Energy*, 29 (2004) 307
5. S. Yang, S. Han, J.Z. Song, Y. Li, *J. Rare Earth*, 29 (2011) 692
6. W.K. Hu, *J. Alloys Compd.*, 289 (1999) 299
7. K. Komori, O. Yamamoto, Y. Toyoguchi, K. Suzuki, S. Yamaguchi, A. Tanaka, M. Ikoma, US5512385 (1996)
8. H. Ye, H. Zhang, W.Q. Wu, T.S. Huang, *J. Alloys Compd.*, 312 (2000) 68
9. Y.H. Zhang, M.Y. Chen, X.L. Wang, G.Q. Wang, X.P. Dong, Y. Qi, *Electrochim. Acta*, 49 (2004) 1161
10. S.Q. Yang, S.M. Han, Y. Li, S.X. Yang, L. Hu, *Mater. Sci. Eng. B* 176 (2010) 231
11. H. Ye, Y.X. Huang, J.X. Chen, H. Zhang, *J. Power Sources*, 103 (2002) 293
12. H.Z. Yan, F.Q. Kong, W. Xiong, B.Q. Li, J. Li, L. Wang, *Int. J. Hydrogen Energy*, 35 (2010) 5687
13. Y. Zhou, Y.Q. Lei, Y.C. Luo, S.A. Cheng, Q.D. Wang, *Acta Metall. Sin.*, 32 (1996) 857
14. Y.H. Zhang, M.Y. Chen, X.L. Wang, G.Q. Wang, X.P. Dong, Y. Qi, *Electrochim. Acta*, 49 (2004) 1161
15. P. Li, X.L. Wang, Y.H. Zhang, R. Li, J.M. Wu, X.H. Qu, *J. Alloys Compd.*, 353 (2003) 278
16. B.Z. Liu, M.J. Hu, L.Q. Ji, Y.P. Fan, Y.G. Wang, Z. Zhang, A.M. Li, *J. Alloys Compd.*, 516 (2012) 53
17. R. Brateng, S. Gulbrandsen-Dahl, L.O. Vaøen, J.K. Solberg, R. Tunold, *J. Alloys Compd.*, 396 (2005) 100
18. X.B. Zhang, D.Z. Sun, W.Y. Yin, Y.J. Chai, M.S. Zhao, *Chem Phys Chem*, 6 (2005) 520
19. P.H.L. Notten, P. Hokkeling, *J. Electrochem. Soc.*, 138 (1991) 1877
20. G. Zheng, B.N. Popov, R.E. White, *J. Electrochem. Soc.*, 142 (1995) 2695
21. C. Iwakura, T. Oura, H. Inoue, M. Matsuoka, *Electrochim. Acta*, 41 (1996) 117
22. C. Iwakura, M. Miyamoto, H. Inoue, M. Matsuoka, Y. Fukumoto, *J. Alloys Compd.*, 259 (1997) 132
23. D. Chartouni, F. Meli, A. Zuttel, K. Gross, L. Schlapbach, *J. Alloys Compd.*, 241 (1996) 160
24. M. Takao, S. Satoshi, S. Naofumi, European Patent 1,075,032, A1 (2001).